Contribution of Carbonyl Photochemistry to Aging of Atmospheric Secondary Organic Aerosol

Stephen A. Mang, Dana K. Henricksen, Adam P. Bateman, Mads P. Sulbaek Andersen, Donald R. Blake, and Sergey A. Nizkorodov*

Department of Chemistry, University of California, Irvine, California 92697

Received: May 17, 2008; Revised Manuscript Received: July 3, 2008

The photodegradation of secondary organic aerosol (SOA) material by actinic UV radiation was investigated. SOA was generated via the dark reaction of ozone and *d*-limonene, collected onto quartz-fiber filters, and exposed to wavelength-tunable radiation. Photochemical production of CO was monitored in situ by infrared cavity ring-down spectroscopy. A number of additional gas-phase products of SOA photodegradation were observed by gas chromatography, including methane, ethene, acetaldehyde, acetone, methanol, and 1-butene. The absorption spectrum of SOA material collected onto CaF_2 windows was measured and compared with the photolysis action spectrum for the release of CO, a marker for Norrish type-I photocleavage of carbonyls. Both spectra had a band at ~300 nm corresponding to the overlapping $n \rightarrow \pi^*$ transitions in nonconjugated carbonyls. The effective extinction coefficient of freshly prepared SOA was estimated to be on the order of 15 L mol^{-1} cm^{-1} at 300 nm, implying one carbonyl group in every SOA constituent. The absorption by the SOA material slowly increased in the visible and near-UV during storage of SOA in open air in the dark, presumably as a result of condensation reactions that increased the degree of conjugation in the SOA constituents. These observations suggest that photolysis of carbonyl functional groups represents a significant sink for monoterpene SOA compounds in the troposphere, with an estimated lifetime of several hours over the continental United States.

1. Introduction

The importance of secondary organic aerosols (SOA) formed from biogenic and anthropogenic precursors has become recognized in recent years.[1] Globally, SOA production is predicted to amount to 120−910 Tg/year,[2−4] with most of this highly uncertain amount coming from oxidation of volatile organic compounds (VOCs) by O_3, OH, and NO_3. It is generally believed that 90% of the SOA burden is due to the oxidation of biogenic VOCs,[1] of which as much as 63 Tg carbon per year may come from the oxidation of isoprene (C_5H_8) and monoterpenes ($C_{10}H_{16}$). Semivolatile components of primary organic aerosols can also be oxidized, further contributing to the secondary aerosol burden in polluted areas.[3] The substantial uncertainty in the amount of SOA produced yearly comes in part from an incomplete understanding of how SOA formation from biogenic VOC oxidation depends on environmental conditions.

Understanding the aging processes that modify SOA composition after its initial formation is also incomplete.[5] There are several ways in which the composition of an atmospheric organic particle can be modified. In terms of chemical modifications, the composition can be altered by reactive uptake of atmospheric oxidants at the particle's surface[5−7] and by the irreversible partitioning of certain VOCs to the particle phase.[8,9] The observation of time evolution of the oligomer content in SOA suggests that condensed-phase reactions in particles also play a role in slowly altering the aerosol composition.[10−12]

Direct and indirect photochemical processes can also contribute to aging of organic aerosol.[13−15] The former include direct photodissociation of organic molecules in the particle phase, whereas the latter include gas-phase photochemical oxidation of semivolatiles that temporarily desorbed from the particle phase and condensed back after the oxidation.[3] It is known that organic molecules in fog waters undergo degradation by exposure to sunlight on atmospherically relevant time scales.[16−18] Efficient photochemical degradation of PAHs has also been observed in combustion-derived particles.[13,19,20] Because typical atmospheric lifetimes for fine organic particles are on the order of several days, photodegradation of SOA constituents with actinic radiation ($\lambda > 300$ nm) is likely to be significant as well.

Previous research in our group has focused on the role played by direct photodissociation of organic peroxides in the photochemical aging of SOA produced by ozone-initiated oxidation of *d*-limonene.[15] In this work, we describe a new set of experiments that further explores photochemical aging of *d*-limonene SOA. A combination of techniques including infrared cavity ring-down spectroscopy (IR-CRDS), gas chromatography (GC), and UV/vis absorption spectroscopy are used to provide insight into the role of carbonyl photochemistry in SOA aging mechanisms.

2. Experimental Section

2.1. Particle Production and Collection. SOA was produced from the reaction of *d*-limonene (Sigma-Aldrich, ≥98%) with ozone in a 250 L Teflon chamber as described previously.[15] Reactions were conducted in the dark at ~750 Torr, ~298 K, and low relative humidity (<1%). Ozone was added to the chamber first, by flowing high-purity (99.994%) oxygen through a commercial ozone generator. This was followed by an injection of several microliters of *d*-limonene into the chamber with a syringe. In order to accelerate the reaction and improve

* Corresponding author. E-mail: nizkorod@uci.edu.

10.1021/jp804376c CCC: $40.75
Published on Web 08/14/2008

the SOA yield, a large excess of ozone was used. Typical initial reagent concentrations were 300 ppm ozone and 10 ppm *d*-limonene (97%, Fisher Scientific). Although these concentrations are high compared to what would be found in the troposphere, the ratio of *d*-limonene to ozone concentration is close to that observed under nocturnal conditions.[21] In several experiments, SOA was prepared at lower concentrations (1 ppm O_3, 500 ppb *d*-limonene) to test whether the results of the photodegradation experiments were concentration-dependent.

Particle collection commenced 10 min after the *d*-limonene injection. For GC experiments, particles were collected by pumping 2.0 standard liters per minute (SLM) of chamber air through 47 mm diameter glass fiber filters mounted in Millipore stainless-steel filter holders for 60 min. For IR-CRDS experiments, particles were collected onto six identical 10 mm glass fiber filters in parallel, with 1.0 SLM air drawn through each filter for 30 min. Prior to collection, all glass fiber filters (0.7 μm average pore size) were baked overnight to remove organic contamination. For UV/vis absorption spectroscopy, particles were collected onto two 2.5 cm diameter CaF_2 windows in parallel using single-jet impactors (PIXE International Corp., 0.12 μm effective particle diameter cutoff) operated at 1.0 SLM for 60 min (longer in the case of low-concentration experiments). In all cases, an oil-free pump (Hi-Q Environmental, 1023CV) was used for collection. The pump inlet was split into six independent branches, each equipped with a calibrated flow meter to regulate the pumping rate. Filters and windows were weighed before and after particle collection using a filter microbalance (Sartorius ME5-F, $\sim$2 μg accuracy) in order to determine the amount of collected SOA material.

2.2. UV/vis Absorption Spectroscopy. SOA material was collected on CaF_2 windows and analyzed in a dual-beam UV/vis spectrometer (Shimadzu, UV-2450). The largest amount of collected SOA material was concentrated by the impaction process in a $\sim$2 mm opaque ring located in the center of the window. In order to create a more uniform and optically thin film, two CaF_2 windows containing SOA material were pressed together and rotated several times. This resulted in the aerosol material being spread more evenly over roughly a third of the window area. Gently heating the windows made it possible to spread the material in a visibly uniform film over the entire window surface. The windows were separated, weighed to determine the mass of the SOA film, and attached to the ends of a 5 cm absorption cell with O-ring seals to make it possible to flow clean air over the SOA film while it was sitting inside the spectrometer. Spectra were measured relative to two clean CaF_2 windows. Because of a refractive index mismatch between CaF_2 and SOA, the measured absorbance was reproducibly shifted from zero by an amount that was nearly constant over the entire visible and near-IR range. Approximate corrections for the refractive index mismatch were applied using a wavelength-independent refractive index of SOA material as an adjustable parameter. A refractive index in the range of 1.4−1.5 for the SOA material gave the best results. In addition, for SOA samples that were not spread over a sufficiently large area, a small shift in absorbance appeared because of scattering of the spectrometer light on the nonuniformities of the SOA film. This shift was subtracted to make the absorbance at 700 nm equal to zero. UV/vis spectra were recorded immediately after collection and then periodically for up to 72 h afterward to monitor changes in absorption with time.

2.3. SOA Photodegradation Analyzed by IR-CRDS. The IR-CRDS instrument used in this work has been described in detail elsewhere.[14] In this work, the CRDS mirrors were replaced by a set optimized for the 4.5 μm wavelength range (R> 99.98%, Los Gatos Research) to enable detection of the CO fundamental vibrational band. The cavity was pumped by an optical parametric oscillator laser (LaserVision), which was in turn pumped by a pulsed Nd:YAG laser (Continuum Powerlite 8000). A Teflon filter holder containing the SOA sample was placed in the cavity just below the pulsed IR beam, and appropriately filtered UV radiation from a Xenon lamp illuminator (Oriel PhotoMax) was directed onto the sample. For wavelength-dependence experiments, the UV radiation was first sent through a monochromator (Spectra Physics Cornerstone 1/8 m). The slits of the monochromator were wide open, resulting in 3−20 mW of 10 nm bandwidth of radiation passing through. For each batch of SOA filters, photolysis at six different wavelengths could be examined (one filter per wavelength). One of these wavelengths was always 280 nm for normalization purposes. Photolysis experiments were conducted under conditions of ultrahigh-purity (UHP, 99.999%) He flow at $\sim$100 Torr, with $\sim$1 s residence time in the CRDS cavity. Heating of the filter by absorbed UV radiation was negligible (<2 °C).

2.4. SOA Photodegradation Analyzed by GC. Samples of SOA material were collected onto glass-fiber filters, which were then placed inside a quartz tube (i.d. = 15 mm, length = 30 cm). UHP helium flowed over the sample for 10−30 min at reduced pressure to remove the most volatile species adsorbed to the filter. The tube was then filled to 700 Torr with UHP helium and the sample was photolyzed for 30 min with a Xenon lamp illuminator. The lamp output was first reflected by a 330 nm dichroic mirror and then filtered with a 295 nm high-pass filter. The total radiation power incident on the sample was $\sim$20 mW, which mostly consisted of wavelengths between 300 and 350 nm. Sample heating was negligible over the course of the photolysis (<2 °C). Three modes of blank background samples were prepared under similar conditions: type 1, irradiation of clean filter for 30 min; type 2, clean filter in darkness for 30 min; and type 3, SOA-loaded filter in darkness for 30 min. Background VOC levels in all type-1 and -2 samples were at or below the levels found in type-3 samples.

The gaseous photolysis products were collected into conditioned, evacuated 2 L stainless-steel canisters each equipped with a bellows valve and pressurized to 650 Torr with pure He diluent. The canisters were promptly analyzed upon collection. Samples were cryogenically trapped and injected into a multicolumn/detector gas chromatography system for VOC detection. The detectors included flame ionization detectors (FID), electron capture detectors (ECD), and a quadrupole mass spectrometer (MSD). Four different column/detector combinations were used: PLOT/FID, DB-1/FID, DB-5+Restek 1701/ECD, and DB-5 ms/MSD. Methane and carbon monoxide were analyzed using separate GC/FID systems, whereas GC with thermal conductivity detection was utilized for analysis of CO_2. The calibration scheme, which was routinely cross-checked against absolute standards from other groups, employed a combination of primary standards and secondary working standards of air collected from different environments and calibrated to certified standards. This analysis allowed accurate quantification of a large variety of different gaseous species.[22]

3. Results

3.1. UV/vis Absorption Spectroscopy. SOA material collected on CaF_2 windows was analyzed immediately after collection to determine its initial absorption profile. The acquisition of UV/vis spectra continued for a period of 72 h afterward to monitor the changes in the spectrum caused by

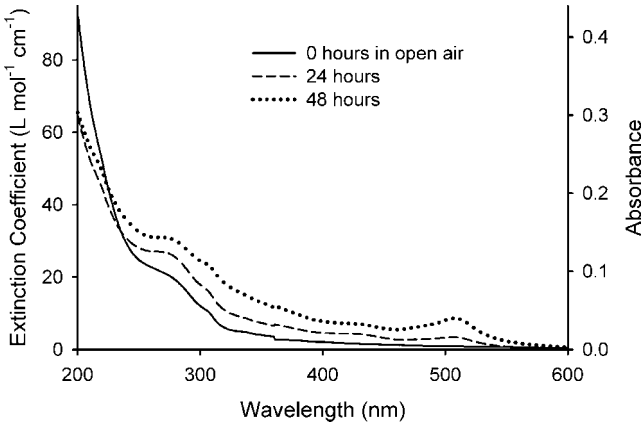

Figure 1. UV/vis absorption spectra of *d*-limonene SOA material collected on a CaF_2 window as a function of storage time. The SOA samples were stored in open air in darkness. The changes in the absorption profile were accompanied by a visible transition of the material from colorless to red-brown.

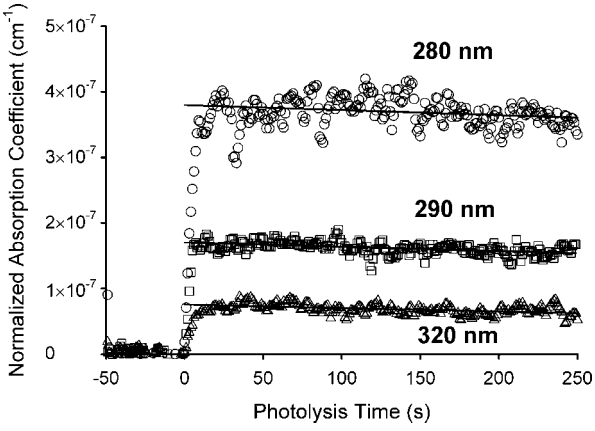

Figure 2. Representative CO signals measured by IR-CRDS at different UV radiation wavelengths as a function of photolysis time. The measured absorption coefficients were normalized by the wavelength-dependent radiation fluxes. The irradiation was initiated at time zero. Lines represent linear least-squares fits to the data after 20 s of photolysis.

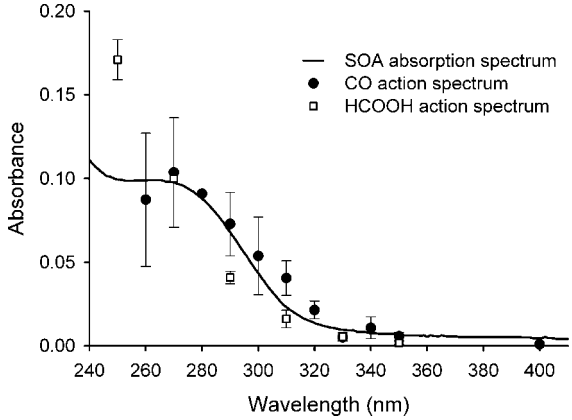

Figure 3. Comparison of the UV/vis absorption spectrum, formic acid action spectrum,[15] and CO action spectrum of *d*-limonene SOA produced under similar conditions.

time spent in open air. The initial absorption spectrum (Figure 1) shows that fresh SOA from *d*-limonene ozonolysis absorbs significantly at wavelengths below ~350 nm. The shape of the absorption profile appears to be dominated by transitions characteristic of peroxy and carbonyl functional groups in SOA which are expected products of ozonolysis of olefins. There is no significant difference in the shape of the absorption profiles for particles prepared at low and high reagent concentrations.

The CaF_2 windows were separated before analysis, continuously exposing the SOA films on the windows to the clean air flow. These SOA samples, as well as those collected on glass-fiber filters, showed a significant change in color from colorless to red-brown after about a day spent in open air in the dark (~50% RH, 298 K). Changes in the absorption profile continued even after any further visible color change became imperceptible and were still ongoing after 72 h in the dark in ambient air (Figure 1). The color change slowed down significantly in dry air. For example, when the fresh SOA samples were left on CaF_2 windows under dry nitrogen, no significant color change was observed after two days. If the same samples were removed from the nitrogen atmosphere and exposed to room air, the color changes reappeared. To avoid complications associated with these aging effects, all photolysis experiments described below used fresh SOA samples (<6 h old) that were not exposed to ambient air.

3.2. IR-CRDS Measurements. The production of CO during photodegradation of *d*-limonene SOA was explicitly confirmed by scanning the IR laser over the $v = 1 \leftarrow 0$ vibrational band of CO while irradiating the SOA sample at actinic UV wavelengths (between 300 and 350 nm). The scan produced a rotationally resolved spectrum of CO, with clearly resolved P and R branches. The irradiation did not produce a significant increase in the unresolved background between the CO ro-vibrational lines. Photochemical CO production was observed for SOA samples generated under both high and low ozone-concentration conditions.

To examine the relative yield of CO at different UV excitation wavelengths, the IR laser was fixed on top of the R(6) line of the $v = 1 \leftarrow 0$ band of CO at 2169.2 cm^{-1} while the UV excitation wavelength was varied. Figure 2 shows the relative CO production as a function of photolysis time at various UV wavelengths, expressed in terms of the absorption coefficient, α. This coefficient was calculated from the cavity ring-down time measured in the presence and absence of the UV radiation,

$$\alpha = \frac{1}{c}\left(\frac{1}{\tau} - \frac{1}{\tau_0}\right) \quad (1)$$

where c is the speed of light, τ is the ring-down time with the radiation present, and τ_0 is the ring-down time of an empty cavity. The calculated absorption coefficient was further normalized by the relative UV radiation flux (the number of photons hitting the sample per second) to account for the variations in the transmitted lamp power as a function of wavelength. The relative UV radiation flux at 280 nm was arbitrarily set equal to 1. The ratio between the normalized and actual absorption coefficients in Figure 2 is less than a factor of 3.

The time-dependent signals shown in Figure 2 were extrapolated to time = 0 (the time at which the UV exposure started) to obtain the initial CO yields. This backward regression helps to account for the slow photobleaching of SOA samples by the UV radiation. Figure 3 shows the resulting relative yield of CO as a function of the irradiation wavelength. Error bars represent one standard deviation from averaging multiple independent experiments with different SOA batches. There is no error bar at 280 nm because all yields were measured relative to this point. The largest relative CO yield was observed at 270−280 nm, but there was clear evidence of photolysis resulting in CO production above 300 nm. Above 400 nm, the CO signal dropped below the detection limits of the CRDS instrument. For comparison, the UV/vis absorption spectrum of *d*-limonene

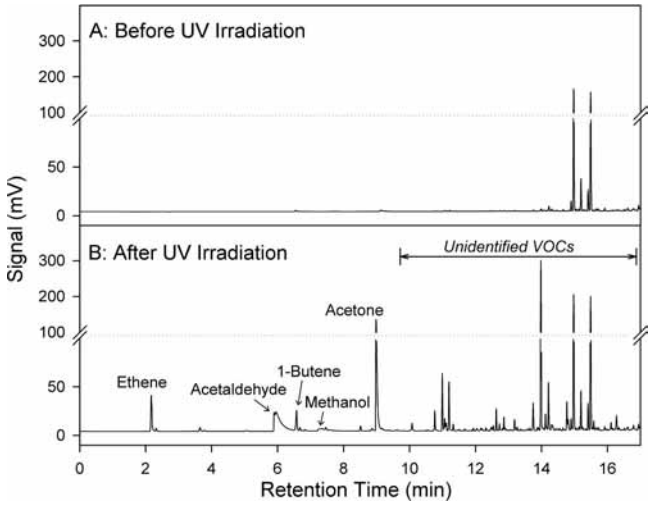

Figure 4. Sample GC traces, obtained using a DB-1/FID column/detector combination, of headspace gas above the SOA filter before (A) and after (B) UV irradiation (300−350 nm).

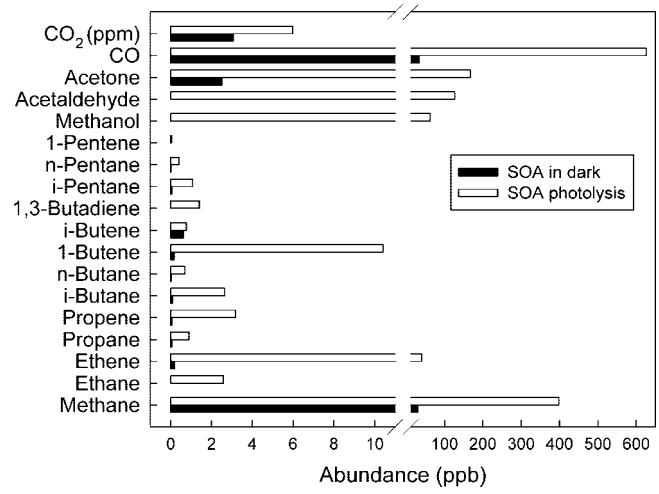

Figure 5. Relative amounts of selected VOCs observed in the headspace gas above the SOA filter before (dark bars) and after (white bars) irradiation at 300−350 nm. The CO_2 mixing ratio is in ppm, and the remaining mixing ratios are in ppb. Note the change of scale after the break.

SOA and a formic acid action spectrum from similarly prepared SOA samples[15] are presented in Figure 3 as well.

3.3. GC Measurements. The GC system used in this experiment made it possible to measure the relative amounts of CO, CO_2, CH_4, and various hydrocarbons, aldehydes, ketones, and alcohols among the SOA photodegradation products. Figure 4 shows representative gas chromatograms obtained using a DB-1 column and FID detector combination for SOA samples produced under high reactant concentrations (300 ppm ozone, 10 ppm *d*-limonene). Panel A in Figure 4 shows a chromatogram obtained for the headspace gas above the SOA filter before exposure to any radiation. Panel B shows a chromatogram recorded after the UV exposure. Comparison of panels A and B reveals numerous gaseous photodegradation products that either appeared or increased substantially in concentration after the irradiation. Although the majority of the peaks defied assignment, several of them could be assigned to specific molecules on the basis of explicit comparison with VOC standards. For example, Figure 4 has significant peaks corresponding to ethene, acetaldehyde, 1-butene, methanol, ethanol, and acetone. Figure 5 shows the absolute mixing ratios of all assignable SOA photodegradation products presented as a histogram. CO and CH_4 were the most abundant identified gas-phase products. CO_2 increased in concentration after the irradiation, but it was also observed in the background samples. A large number of unidentified, high molecular-weight oxygenated species were observed at longer elution times.

The experiments were repeated with SOA samples produced at lower concentrations (1 ppm ozone, 0.5 ppm *d*-limonene) to examine the effect of reactant concentrations on the photolysis products. In a typical experiment, 140 μg of SOA were collected from the low-concentration particle generation, compared to 350 μg or more from the high-concentration particle generation. Photolysis of the low-concentration SOA produced the same volatile photoproducts as the high-concentration SOA. The absolute amounts were reduced as expected; however, no drastic change in the relative distribution of products was observed.

4. Discussion

4.1. Absorption Spectra of SOA Material. The UV/vis spectrum of the SOA material represents a convolution of absorption spectra of hundreds of different molecules. Nevertheless, it carries useful information about the average functional makeup of the SOA constituents. For example, a weak transition visible in the *d*-limonene SOA absorption spectrum around 280 nm is consistent with overlapping n $\rightarrow \pi^*$ transitions in nonconjugated aldehydes and ketones,[23] which are expected products of monoterpene ozonolysis. Indeed, multiple products containing nonconjugated carbonyl functional groups have previously been detected in *d*-limonene SOA.[24−27] Examples of important carbonyl constituents of *d*-limonene SOA are listed in Table 1 and shown in Figure 6. They are named on the basis of the convention described in ref 28.

The observed smooth decay of the absorption spectrum between 250 and 350 nm is most likely due to overlapping n $\rightarrow \sigma^*$ transitions in organic peroxides. Peroxides can account for a significant fraction of SOA material produced by ozonolysis of monoterpenes.[29−31] Specifically, ozonolysis of *d*-limonene was shown to produce H_2O_2,[32] as well as various organic peroxides including peroxy hemiacetals, peroxide esters, and secondary ozonides.[33,34] We previously showed that secondary ozonides in *d*-limonene SOA can be photolyzed to produce formic acid and formaldehyde.[15]

The absorption spectra of a known mass of SOA material can be used to estimate the effective (average) extinction coefficients of the SOA molecular constituents. The measured extinction should be dominated by absorption, not scattering, because individual particles in the collected SOA samples are sintered into a film. Furthermore, the reflection losses caused by the mismatch between refractive index of the SOA film and the CaF_2 windows are explicitly subtracted. The extinction coefficient ε (in L mol^{-1} cm^{-1}) is calculated from measured base-10 absorbance A by using Beer's Law, $A = \varepsilon Cx$. The average concentration C (mol L^{-1}) of SOA molecular constituents is calculated by assuming that the SOA material has an average density of 1.5 g cm^{-3} (adopted from ref 35) and consists of molecules with an average molecular weight of 200 g/mol (estimated from mass-spectra of *d*-limonene SOA reported in ref 36). The effective path length x is estimated from the measurements of the area over which the particles are spread and from the gravimetrically determined mass of the collected SOA sample (for example, for a 450 μg SOA sample spread over 0.5 cm^2 area, the effective path length is $\sim$6 μm).

Using these admittedly crude approximations, a 300 nm extinction coefficient of $\varepsilon = 13.5 \pm 1.4$ L mol^{-1} cm^{-1} is

TABLE 1: Expected and Observed Gas-Phase Products (<4 Carbon Atoms) from the Photolysis of Known Major Constituents of *d*-Limonene SOA in an Anoxic Environment[a]

carbonyl-containing constituent of *d*-limonene SOA	expected volatile products of SOA photolysis	
	observed	not observed
limononaldehyde	CO, CH_2O, CH_4, Aa, Ac	
keto-limononaldehyde	CO, CH_2O, CH_4, Aa, Ac	3-buten-2-one
7-hydroxy-limononaldehyde	CO, CH_2O, MeOH, Aa	hydroxyl-Aa, 4-hydroxy-2-butanone
7-hydroxy-keto-limononaldehyde	CO, CH_2O, CH_4, MeOH, Aa	hydroxyl-Ac, hydroxyl-Aa, 1-hydroxy-2-butanone
limononic acid	CO, CH_4, Aa, Ac	
keto-limononic acid	CO, CH_4, Aa, Ac	3-buten-2-one
nor-limononic acid	CO, CH_4, Aa, Ac	
7-hydroxy-limononic acid	CO, MeOH	hydroxyl-Aa, hydroxyl-Ac
7-hydroxy-keto-limononic acid	CO, CH_4, Aa, MeOH	hydroxyl-Aa, hydroxyl-Ac, 1-hydroxy-3-buten-2-one
limonalic acid	CO, CH_2O, Aa	
keto-limonalic acid	CO, CH_2O, CH_4, Aa	acrylic acid
keto-limonic acid	CO, CH_4, Aa	acrylic acid, acetic acid

[a] CO and formaldehyde were observed with both GC and IR-CRDS methods, whereas the remaining identified photodegradation products were detected by GC only. Key: Aa, acetaldehyde; Ac, acetone; MeOH, methanol.

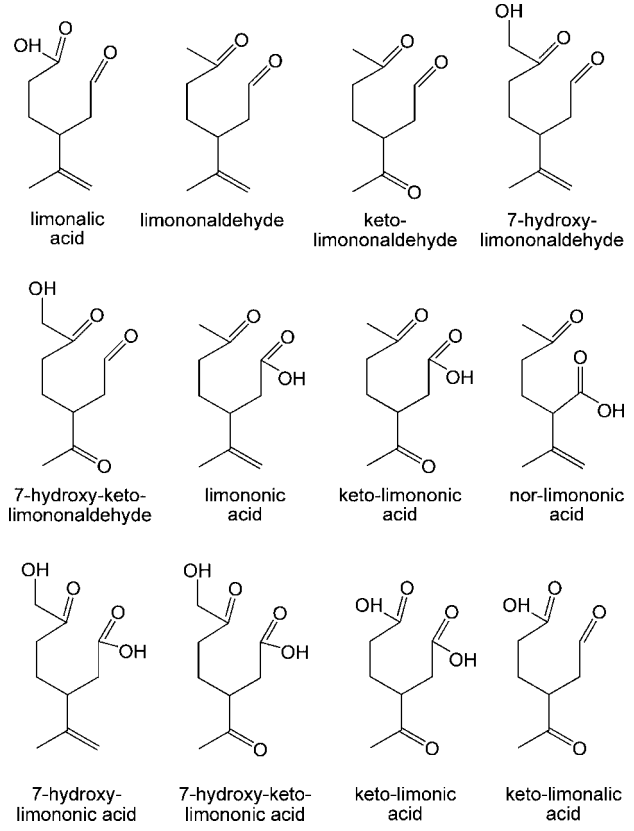

Figure 6. Known major constituents of *d*-limonene SOA containing carbonyl groups. Molecules are named according to conventions of ref 28.

obtained for fresh SOA material. The uncertainties represent one standard deviation resulting from averaging repeated experiments for several SOA samples prepared at high (300 ppm) and low (1 ppm) ozone concentration. They do not include uncertainties associated with the approximations described above. This value is within the typical range for $n \rightarrow \pi^*$ transitions of carbonyl-containing molecules,[37] suggesting that on average, every SOA constituent has one carbonyl group. This conclusion is fully consistent with the mechanism of oxidation of *d*-limonene by ozone. Cycloaddition of ozone to the more reactive endo double bond in *d*-limonene results in a primary ozonide, which quickly decomposes by breaking the *d*-limonene 6-membered ring open. One end of the broken ring is decorated with a carbonyl group, whereas the other is terminated with a carbonyl oxide, which reacts further to produce either a carboxylic acid, carbonyl, or peroxide functionality.[36] The apparent lack of a strong dependence of the measured extinction coefficients on the ozone concentration used in SOA preparation is reasonable because the fraction of the carbonyls produced by this mechanism is not expected to depend on the concentration.

Over the course of two days spent on a CaF_2 window in particle-free air in the dark, the measured extinction coefficient changes dramatically. It increases to some extent at all wavelengths below 550 nm, and new absorption peaks grow in at ~510 and ~430 nm. These peaks achieve an extinction coefficient of $\varepsilon \approx 10$ L mol^{-1} cm^{-1} after two days, whereas the extinction coefficient at 300 nm increases to $\varepsilon \approx 100$ L mol^{-1} cm^{-1}. This increase in the visible and near-UV absorption suggests that condensation reactions between SOA constituents result in increased conjugation in aged SOA. The condensation mechanism is consistent with our observation that SOA material becomes visibly wetted, presumably from water released during the condensation reactions. One possible scenario is aldol condensation of SOA aldehydes catalyzed by SOA carboxylic acids. Aldol condensation has previously been implicated in the large increase in the UV/vis absorption index of sulfuric acid solutions exposed to aliphatic aldehydes.[38−40] We hypothesize that similar processes are at work in SOA material.

The reproducible appearance of a well-defined band at 510 nm is especially intriguing. Examples of absorbing systems that have well-defined transitions in the vicinity of 510 nm and involve only carbon, oxygen, and hydrogen atoms are actually quite limited. Examples include polycyclic aromatic hydrocarbons with 6−9 conjugated rings and quinonoid systems based on 2−3 conjugated rings.[41] Although the former class of absorbers is unlikely to form spontaneously inside the SOA matrix, formation of quinones is plausible because they are known to form from linear polyketones,[42] that is, exactly the sort of products formed by extensive oxidation of cyclic olefins by ozone. These observations certainly warrant further investigation.

4.2. Mechanism of SOA Photodegradation. The $n \rightarrow \pi^*$ transitions in carbonyls are known to lead to photocleavage via Norrish type-I and -II mechanisms.[23,43] In the type-I process, the carbonyl dissociates into two radicals via breaking of the C−C bond between the carbonyl and α carbons:

$$RC(O)R' + h\nu \rightarrow R\bullet + R'C(O)\bullet \qquad (2)$$

All photodegradation experiments discussed in this work have been conducted in UHP helium. Under these anoxic conditions, the free radical containing the carbonyl group can either

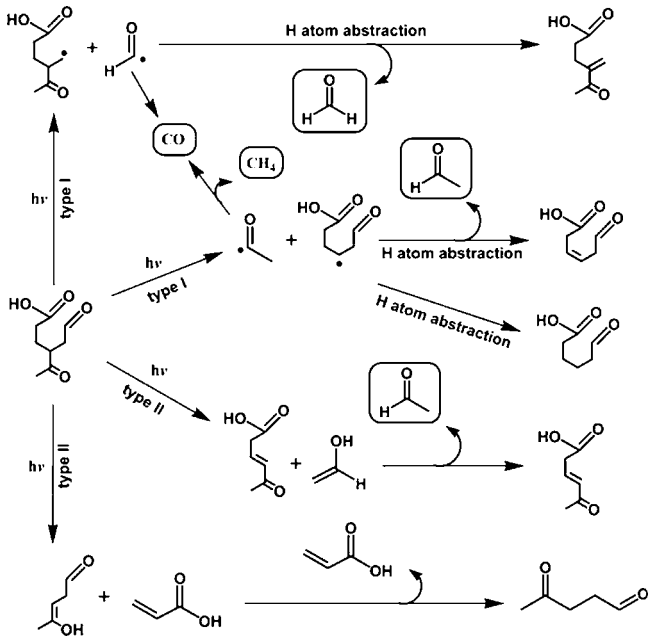

Figure 7. Likely pathways for the photolysis of keto-limonalic acid, a representative component of SOA from *d*-limonene ozonolysis. The photolysis is conducted in the absence of molecular oxygen. For simplicity, only selected Norrish type-I and -II photocleavage pathways are shown.

decarbonylate, resulting in an alkyl radical and carbon monoxide, or abstract a hydrogen atom from another molecule to give an aldehyde.

$$R'C(O)\bullet \rightarrow R'\bullet + CO \quad (3)$$

$$R'C(O)\bullet + R''H \rightarrow R'C(O)H + R''\bullet \quad (4)$$

The Norrish type-II reaction is an intermolecular reaction that cleaves the C−C bond between the α and β carbons and results in the formation of a smaller ketone and an alkene:

$$RR'CHCH_2CH_2C(O)R'' + h\nu \rightarrow RR'C{=}CH_2 + CH_3C(O)R'' \quad (5)$$

This reaction proceeds through a six-membered cyclic intermediate and requires a γ hydrogen atom because this atom is abstracted during the reaction.[44,45]

Carbon monoxide is a unique marker for the type-I photocleavage of carbonyls, whereas type-II processes tend to produce smaller carbonyls and olefins. Comparison of the action spectrum for the photoemission of CO with the absorption spectrum of the SOA material (Figure 3) is consistent with CO production from carbonyl photochemistry. The n → π^* band centered at ∼300 nm is discernible in both the absorption spectrum of SOA and the CO action spectrum, in agreement with its assignment to the carbonyl functional group. In contrast, the shape of the HCOOH action spectrum is quite different. It is consistent with n → σ^* absorption by peroxides, which are characterized by absorption cross sections that decay exponentially with wavelength.[15]

The two Norrish processes can account for a number of the observed SOA photodegradation products. For example, Figure 7 shows selected type-I and-II processes in keto-limonalic acid, a representative component of SOA from *d*-limonene ozonolysis.[24] The volatile products in boxes have been directly observed in this work by GC and CRDS. Table 1 lists expected small VOC products from type-I and-II photolysis of the most common particle phase products from *d*-limonene ozonolysis. Carbon monoxide is an expected product from type-I photolysis of each of these molecules, accounting for its large relative yield (Figure 5). Methane, another observed major product, is a marker for the type-I photolysis of compounds with a 7-methyl group, for example, limononic acid. Formaldehyde is produced from the type-I photolysis of aldehydes as well as from the photolysis of secondary ozonides as previously described.[15] Other observed products include acetaldehyde (produced from type-I photolysis of ketones and type-II photolysis of aldehydes), methanol (a result of hydrogen abstraction by a radical from type-I photolysis of molecules with a 7-hydroxy group, for example, 7-OH-limononic acid), and acetone (from type-II photolysis of molecules with a 7-methyl group).

Short-chain alkenes, such as ethene, were observed as major photodegradation products, but these alkenes cannot be produced directly by the Norrish photocleavage of any of the carbonyls listed in Table 1. However, secondary photolysis of the primary photolysis products can account for the presence of ethene as well as several other olefinic products. Specifically, photolysis of keto-limononaldehyde and keto-limononic acid can produce 3-butene-2-one via type-I photocleavage. Secondary type-I photolysis of 3-butene-2-one generates ethene. The secondary photolysis can occur directly in the SOA matrix before the primary photolysis products desorb from it. The desorption time for oxygenated products can be as long as 10−20 min (we directly measured this time by a chemical ionization mass spectrometer in a separate set of experiments), and it increases with the mass of collected SOA material. Therefore, we expect the GC samples to contain both primary and secondary photolysis products that have accumulated in the gas phase during the 30 min of SOA sample irradiation. For the actual organic particles in the atmosphere with submicron dimensions, desorption of the primary photodegradation products would be much faster. In this case, the secondary photolysis of primary photodegradation products such as methyl ethyl ketone would occur in the gas phase instead of the particle phase.

The chromatogram shown in Figure 4 contains a large number of peaks at long retention times. These peaks likely correspond to oxygenated products containing four or more carbon atoms. A lack of standards for these molecules precluded their identification, but it is possible that some of the peaks are due to high molecular weight photolysis products, similar to those shown in Figure 7. For example, 4-oxopentanal, a product of the type-II photocleavage of keto-limonalic acid (Figure 7), 7-hydroxy-keto-limonalic acid, keto-limonaldehyde, and 7-hydroxy-keto-limonaldehyde, is likely to make its way into the gas phase. 4-Oxopentanal is a known product of reactive loss from ozone on the surfaces of foliage[46] and has been measured over forest areas in both the gas and particle phases.[47] Our data suggest that photodegradation of SOA constituents can also serve as a source of particulate 4-oxopentanal and similar species.

The photodegradation experiments described here have been conducted in an atmosphere of UHP helium rather than air in order to minimize the interference of impurities (especially that of carbon monoxide) and simplify the photochemistry. The nature of the photodegradation products emitted to the gas-phase and left behind in the particle phase will be different in the presence of oxygen. The products of the type-II photolysis will be largely the same, but the products of the type-I process will be significantly altered. In the absence of oxygen, the most likely fate for the free radicals formed in reactions (2−4) is recombination or hydrogen atom abstraction. In the presence of oxygen, these radicals may instead react with molecular oxygen

dissolved in the SOA matrix to form alkylperoxy radicals. These will go on to form various oxygenated molecular products by the well-understood solution phase chemistry of alkylperoxy radicals.[48]

4.3. Atmospheric Lifetimes of Carbonyls in SOA. We can use the measured effective extinction coefficients to estimate the lifetime of carbonyls in SOA with respect to photolysis under typical daytime conditions. The photolysis lifetime, τ_p, of any SOA constituent is the inverse of its photolysis rate constant.[49]

$$(\tau_p)^{-1} = \int_\lambda \sigma(\lambda)\, \phi(\lambda)\, F(\lambda)\, d\lambda \quad (6)$$

where $\sigma(\lambda)$ is the absorption cross section, $\phi(\lambda)$ is the photolysis quantum yield, and F(λ) is the actinic flux. The effective (base-e) absorption cross sections can be calculated from the measured (base-10) extinction coefficients of SOA (Figure 1) by assuming that carbonyls are the primary absorbers above 300 nm. Large carbonyl-containing molecules have quantum yields for photolysis in solution that are always less than unity.[50] Research into photodegradation of ketones in hydrocarbon solvents revealed that the quantum yields are substantial for small ketones, but they rapidly decrease with the ketone chain length down to limiting values of 0.01 and 0.06 for the type-I and -II processes, respectively.[51] Furthermore, type-I processes are likely to be suppressed as viscosity of the solvent increases.[52] Primary products of *d*-limonene ozonolysis have 10 carbon atoms, and ketones of this chain length are expected to have quantum yields in the range of ~0.01 for the type-I reactions and ~0.1 for the type-II reactions.[51] For our lifetime calculations, we have assumed an overall, wavelength-independent quantum yield of 0.1 for the photolysis of carbonyls.

Convolution of the experimentally determined absorption cross sections with the actinic flux between 290 and 490 nm (tabulated in ref 49) results in a photolysis lifetime of ~300 min (5 h) for solar zenith angle (SZA) = 10°, which is characteristic of Southern California at noon in July. Similar calculations for Midwestern United States in summer (for example, St. Louis, Missouri, SZA = 20°) result in $\tau_p \approx 6$ h. The lifetime increases to ~8.3 h in the case of 60° SZA, as it would exist in Atlanta, Georgia at 6 pm in July. In the extreme case of 86° SZA, when no radiation at wavelengths shorter than 315 nm penetrates to the surface, the lifetime increases to ~100 h because of the much smaller overlap between the absorption profile and the actinic radiation flux.

The estimated photolysis lifetimes for small SZA are approximately an order of magnitude smaller than the expected lifetime with respect to aging due to surface oxidation of organic particles by OH (~30 h for an uptake coefficient of 0.1 and a typical atmospheric concentration of [OH] = 10^6 molecules cm^{-3}).[5] Additionally, OH attack will primarily affect the molecules on the surface of SOA particles, whereas photolysis has the potential to age molecules throughout the particle volume.

5. Conclusions

The combination of absorption and photodissociation spectroscopy of films of SOA material produced from *d*-limonene ozonolysis confirms that SOA is susceptible to photochemical aging in the tropospheric actinic region. Carbonyl functional groups are significant players in this aging, as evidenced by the production of large quantities of CO, CH_4, acetaldehyde, acetone, and other VOCs during photodegradation of SOA carbonyl constituents. Many of these products can be explained by standard Norrish type-I and -II photochemistry of carbonyls. The estimated lifetimes of SOA carbonyls with respect to photolysis are on the order of several hours, indicating that this should be considered an important aging process for atmospheric SOA. There is a competing aging process that occurs in the dark and leads to an increase in visible and near-UV absorption by the SOA constituents. The mechanism of this aging process is likely to involve slow condensation reactions of SOA constituents that result in molecules with a high degree of double-bond conjugation, quite possibly with quinonoid structures.

Acknowledgment. This study was supported by the National Science Foundation through the Environmental Molecular Science Institute program, Grant CHE-0431312, and Atmospheric Chemistry program, Grant ATM-0509248.

References and Notes

(1) Kanakidou, M.; Seinfeld, J. H.; Pandis, S. N.; Barnes, I.; Dentener, F. J.; Facchini, M. C.; Van Dingenen, R.; Ervens, B.; Nenes, A.; Nielsen, C. J.; Swietlicki, E.; Putaud, J. P.; Balkanski, Y.; Fuzzi, S.; Horth, J.; Moortgat, G. K.; Winterhalter, R.; Myhre, C. E. L.; Tsigaridis, K.; Vignati, E.; Stephanou, E. G.; Wilson, J. *Atm. Chem. Phys.* **2005**, *5*, 1053–1123.

(2) Chung, S. H.; Seinfeld, J. H. *J. Geophys. Res. D* **2002**, *107*, 4407.

(3) Robinson, A. L.; Donahue, N. M.; Shrivastava, M. K.; Weitkamp, E. A.; Sage, A. M.; Grieshop, A. P.; Lane, T. E.; Pierce, J. R.; Pandis, S. N. *Science* **2007**, *315*, 1259–1262.

(4) Goldstein, A. H.; Galbally, I. E. *Environ. Sci. Technol.* **2007**, *41*, 1514–1521.

(5) Rudich, Y.; Donahue, N. M.; Mentel, T. F. *Annu. Rev. Phys. Chem.* **2007**, *58*, 321–352.

(6) De Gouw, J. A.; Lovejoy, E. R. *Geophys. Res. Lett.* **1998**, *25*, 931–934.

(7) Rudich, Y. *Chem. Rev.* **2003**, *103*, 5097–5124.

(8) Kroll, J. H.; Ng, N. L.; Murphy, S. M.; Varutbangkul, V.; Flagan, R. C.; Seinfeld, J. H. *J. Geophys. Res. D* **2005**, *110*, D23207.

(9) Hughes, L. S.; Allen, J. O.; Bhave, P.; Kleeman, M. J.; Cass, G. R.; Liu, D. Y.; Fergenson, D. P.; Morrical, B. D.; Prather, K. A. *Environ. Sci. Technol.* **2000**, *34*, 3058–3068.

(10) Sax, M.; Zenobi, R.; Baltensperger, U.; Kalberer, M. *Aerosol Sci. Technol.* **2005**, *39*, 822–830.

(11) Baltensperger, U.; Kalberer, M.; Dommen, J.; Paulsen, D.; Alfarra, M. R.; Coe, H.; Fisseha, R.; Gascho, A.; Gysel, M.; Nyeki, S.; Sax, M.; Steinbacher, M.; Prevot, A. S. H.; Sjogren, S.; Weingartner, E.; Zenobi, R. *Faraday Discuss.* **2005**, *130*, 265–278.

(12) Surratt, J. D.; Murphy, S. M.; Kroll, J. H.; Ng, N. L.; Hildebrandt, L.; Sorooshian, A.; Szmigielski, R.; Vermeylen, R.; Maenhaut, W.; Claeys, M.; Flagan, R. C.; Seinfeld, J. H. *J. Phys. Chem. A* **2006**, *110*, 9665–9690.

(13) McDow, S. R.; Jang, M.; Hong, Y.; Kamens, R. M. *J. Geophys. Res. D* **1996**, *101*, 19593–19600.

(14) Gomez, A.; Park, J.; Walser, M.; Lin, A.; Nizkorodov, S. A. *J. Phys. Chem. A* **2006**, *110*, 3584–3592.

(15) Walser, M. L.; Park, J.; Gomez, A. L.; Russell, A. R.; Nizkorodov, S. A. *J. Phys. Chem. A* **2007**, *111*, 1907–1913.

(16) Vione, D.; Maurino, V.; Minero, C.; Pelizzetti, E.; Harrison, M. A. J.; Olariu, R.-I.; Arsene, C. *Chem. Soc. Rev.* **2006**, *35*, 441–453.

(17) Anastasio, C.; McGregor, K. G. *Aerosol Sci. Technol.* **2000**, *32*, 106–119.

(18) Zhang, Q.; Anastasio, C. *Environ. Sci. Technol.* **2003**, *37*, 3522–3530.

(19) Fan, Z.; Kamens, R. M.; Hu, J.; Zhang, J.; McDow, S. *Environ. Sci. Technol.* **1996**, *30*, 1358–1364.

(20) Feilberg, A.; Nielsen, T. *Environ. Sci. Technol.* **2001**, *35*, 108–113.

(21) Roberts, J. M.; Hahn, C. J.; Fehsenfeld, F. C.; Warnock, J. M.; Albritton, D. L.; Sievers, R. E. *Environ. Sci. Technol.* **1985**, *19*, 364–369.

(22) Colman, J. J.; Swanson, A. L.; Meinardi, S.; Sive, B. C.; Blake, D. R.; Rowland, F. S. *Anal. Chem.* **2001**, *73*, 3723–3731.

(23) Calvert, J. G.; Pitts, J. N. *Photochemistry*; John Wiley & Sons: New York, 1966.

(24) Glasius, M.; Lahaniati, M.; Calogirou, A.; Di Bella, D.; Jensen, N. R.; Hjorth, J.; Kotzias, D.; Larsen, B. R. *Environ. Sci. Technol.* **2000**, *34*, 1001–1010.

(25) Hakola, H.; Arey, J.; Aschmann, S. M.; Atkinson, R. *J. Atm. Chem.* **1994**, *18*, 75–102.

(26) Grosjean, D.; Williams, E. L., II.; Grosjean, E.; Andino, J. M.; Seinfeld, J. H. *Environ. Sci. Technol.* **1993**, *27*, 2754–2758.

(27) Leungsakul, S.; Jaoui, M.; Kamens, R. M. *Environ. Sci. Technol.* **2005**, *39*, 9583–9594.

(28) Larsen, B. R.; Lahaniati, M.; Calogirou, A.; Kotzias, D. *Chemosphere* **1998**, *37*, 1207–1220.

(29) Tolocka, M. P.; Heaton, K. J.; Dreyfus, M. A.; Wang, S.; Zordan, C. A.; Saul, T. D.; Johnston, M. V. *Environ. Sci. Technol.* **2006**, *40*, 1843–1848.

(30) Docherty, K. S.; Wu, W.; Lim, Y. B.; Ziemann, P. J. *Environ. Sci. Technol.* **2005**, *39*, 4049–4059.

(31) Bonn, B.; Von Kuhlmann, R.; Lawrence, M. G. *Geophys. Res. Lett.* **2004**, *31*, L10108.

(32) Hewitt, C. N.; Kok, G. L. *J. Atm. Chem.* **1991**, *12*, 181–194.

(33) Heaton, K. J.; Dreyfus, M. A.; Wang, S.; Johnston, M. V. *Environ. Sci. Technol.* **2007**, *41*, 6129–6136.

(34) Nojgaard, J. K.; Norgaard, A. W.; Wolkoff, P. *Int. J. Mass Spectrom.* **2007**, *263*, 88–93.

(35) Kostenidou, E.; Pathak, R. K.; Pandis, S. N. *Aerosol Sci. Technol.* **2007**, *41*, 1002–1010.

(36) Walser, M. L.; Dessiaterik, Y.; Laskin, J.; Laskin, A.; Nizkorodov, S. A. *Phys. Chem. Chem. Phys.* **2008**, *10*, 1009–1022.

(37) Coxon, J. M.; B., H. *Organic photochemistry*, 2nd Edition; Cambridge University Press: Cambridge, 1987.

(38) Noziere, B.; Esteve, W. *Atmos. Environ.* **2007**, *41*, 1150–1163.

(39) Noziere, B.; Esteve, W. *Geophys. Res. Lett.* **2005**, *32*, L03812.

(40) Casale, M. T.; Richman, A. R.; Elrod, M. J.; Garland, R. M.; Beaver, M. R.; Tolbert, M. A. *Atmos. Environ.* **2007**, *41*, 6212–6224.

(41) Hirayama, K. *Handbook of Ultraviolet and Visible Absorption Spectra of Organic Compounds*, 2nd ed; Plenum: New York, 1971.

(42) *The Chemistry of the Quinonoid Compounds*; Patai, S.; Rappoport, Z., Eds.; John Wiley & Sons; Chichester, UK, 1988; Vol. 2, Parts 1 and 2.

(43) Norrish, R. G. W.; Bamford, C. H. *Nature* **1936**, *138*, 1016.

(44) Srinivasan, R. *J. Am. Chem. Soc.* **1959**, *81*, 5061–5065.

(45) McMillan, G. R.; Calvert, J. G.; Pitts, J. N., Jr *J. Am. Chem. Soc.* **1964**, *86*, 3602–3605.

(46) Fruekilde, P.; Hjorth, J.; Jensen, N. R.; Kotzias, D.; Larsen, B. *Atmos. Environ.* **1998**, *32*, 1893–1902.

(47) Matsunaga, S.; Mochida, M.; Kawamura, K. *Chemosphere* **2004**, *55*, 1143–1147.

(48) Ingold, K. U. *Acc. Chem. Res.* **1969**, *2*, 1–9.

(49) Finlayson-Pitts, B. J.; Pitts, J. N. *Chemistry of the Upper and Lower Atmosphere: Theory, Experiments, and Applications*; Academic Press: San Diego, 2000.

(50) Robbins, W. K.; Eastman, R. H. *J. Am. Chem. Soc.* **1970**, *92*, 6077–6079.

(51) Hartley, G. H.; Guillet, J. E. *Macromolecules* **1968**, *1*, 413–417.

(52) Hartley, G. H.; Guillet, J. E. *Macromolecules* **1968**, *1*, 165–170.

JP804376C